PHILOSOPHICAL TRANSACTIONS OF THE ROYAL SOCIETY A MATHEMATICAL, PHYSICAL & ENGINEERING SCIENCES

The Dispersion of Pollutants in the Free Atmosphere by the Large Scale Wind Systems

R. J. Murgatroyd

Phil. Trans. R. Soc. Lond. A 1969 **265**, 273-294
doi: 10.1098/rsta.1969.0055

Phil. Trans. Roy. Soc. Lond. A. **265**, 273–294 (1969) [273]
Printed in Great Britain

V. WORLD-WIDE DISPERSAL OF POLLUTANTS

The dispersion of pollutants in the free atmosphere by the large scale wind systems

By R. J. Murgatroyd
Meteorological Office, Bracknell, Berkshire

The travel and dispersion of pollutants in the free atmosphere may be investigated by the direct measurement of the distributions of tracer materials such as water vapour, ozone and radioactive substances. Another method is to study the spread of pollutants from a constant point source or the expansion of large clusters, by using air trajectories found by tracking balloons or estimated from sequences of wind values obtained from synoptic charts. So far these latter techniques have usually only taken horizontal motions into account since the balloons are normally maintained at constant levels and the winds taken from the charts have been assumed to be geostrophic.

In principle the effect of large (synoptic) scale vertical motions can be included by using the component wind fields given at the different time steps of a numerical forecast integration to construct suitable three-dimensional trajectories. A pilot study of this type at the 900, 700, 500 and 300 mbar pressure levels (90, 70, 50 and 30 kN m^{-2}) using the results of a 24 h numerical forecast by the Meteorological Office's 10 level model is described. In the case studied the use of constant level trajectories gave horizontal dispersions (variances of the trajectory end points relative to their centre of gravity) which differed by only small amounts from those due to the three dimensional trajectories. The zonal variances exceeded the meridional variances by a small factor and both were 4 to 6 orders greater than those of the corresponding variances in the vertical. In each case for at least 12 to 18 h they were all roughly proportional to the square of the time after release (the 'short time' case). The large scale clusters rapidly distorted at rates which increased with their initial size and also with the deformation components of the wind field. At these scales deformation plays a major role in the apparent dispersion and the mean values of total deformation so obtained agreed satisfactorily with those calculated from a kinematic analysis of the horizontal wind field.

Introduction

The study of the motion and dispersion of pollutants carried long distances in the Earth's atmosphere and hence acting as tracers of the wind field has added greatly to our knowledge of the general circulation. For example the travel of the dust thrown up by the great Krakatoa explosion of 1883 gave us some of the earliest data on the wind field of the equatorial stratosphere. More recently measured distributions of radioactive substances have supplemented observations of humidity and ozone in the study of transfer mechanisms within and between the stratosphere and the troposphere. Conversely wind measurements have been widely used to construct trajectories and hence infer sources of airborne material. A well known example in the United Kingdom is the 'red-rain' of 1 July 1968 which was attributed to dust transported in the atmosphere from North Africa or Spain. Air trajectory studies of the carriage of dust, pollen, spores, insects, etc., between different countries and even continents have received wide application. In addition, the use of constant level balloons has become an important source of data on large scale atmospheric motions and is being developed as a new technique of global wind measurements.

The atmospheric motions comprise a very wide spectrum ranging from molecular scales through the smallest mechanically produced eddies, convective cells, gravity waves, depressions and anticyclones, to the large scale transient and standing planetary waves and also the global mean circulation cells. This assemblage of motion systems can be regarded as a field of turbulence and two examples of estimates of its overall characteristic energy spectrum are given in figure 1 (see, for example, Van der Hoven 1957; Pinus, Reiter, Shur & Vinnichenko 1967). Eddies with lifetimes of seconds or minutes comprise the 'microturbulence', those lasting for minutes to hours the 'mesoturbulence' and the major depressions, anticyclones, etc., which may be present for days or weeks, the 'macroturbulence'. It is the latter with which this paper is mainly concerned.

The different motion systems are continually changing in time and space but also vary to a large extent in a systematic way with such factors as topography latitude and vertical stability so that atmospheric turbulence is neither stationary nor homogeneous, although these assumptions usually have to be made in the application of existing theory to observations. Dispersion of pollutants by the macroturbulence is usually discussed in terms of the following two cases:

(i) The dispersion of particles from a continuous point source simulated by the spread of the end points of a series of sequential trajectories through a fixed point. The trajectories may be those of constant level balloons or produced from observed or predicted synoptic charts of the wind field. On the global scale it may be possible to apply the results of this type of study to the world wide dispersion of such tracers as ozone, radioactive materials, etc., by the general circulation:

(ii) The relative dispersion of particles in large clusters. In each case the nature and rapidity of the dispersion will depend on the vertical stability as well as on the wind shears and scales of the atmospheric motions concerned. With a continuous point source the displacements of the successive particles relative to fixed axes are determined throughout their travel by all the scales of motion they encounter. The full statistical treatment of the movements due to the whole field of turbulence, however, requires the trajectories to be sufficiently long to obtain a good sample of the effects of all scales including the largest. For a cluster, the rate of spread, i.e. of the relative separation of its particles is determined mainly by the scales of motion which are comparable with the size of the cluster itself. Hence as it grows, successively larger scales of motion play increasingly larger roles. In the following sections the application to macroturbulence of the theoretical framework which has been widely established by studies of dispersion by microturbulence will be discussed for these two cases. In addition the use of numerical models of the atmosphere for investigations of this type will be described and illustrated by a pilot example based on a prediction experiment using the Meteorological Office's 10-level model.

The determination of atmospheric diffusion from trajectories through a fixed point

(a) *Geostrophic trajectory studies*

If a series of synoptic pressure charts at the surface or contour heights of constant pressure surfaces at higher levels are available the instantaneous wind as determined from the geostrophic wind equation can be used to displace a particle for half the time interval to the next chart. Then it can be moved onwards for the whole time interval at the average geostrophic wind speed for the portion of its trajectory on the next chart and so on until a complete trajectory is drawn for the whole of the chart series, usually for a period of a few days. The trajectories so obtained are approximate since they involve averaging in space and time. Improvements in their accuracy can be obtained with some labour by a method of successive approximations (see Petterssen 1956, p. 27). The effect of vertical displacements can also largely be taken into account by using isentropic charts instead of constant pressure charts. When a set of trajectories are constructed and points $x(t)$, $y(t)$ determined on each trajectory for a time t after passing through the source, coordinates of the centre of gravity $\bar{x}(t)$, $\bar{y}(t)$ and also the corresponding variances

$\sigma_x^2(t)$, $\sigma_y^2(t)$ may be found. When t attains a sufficiently large value, T, it may be possible to estimate the eddy diffusivities K_x, K_y by writing

$$K_x = \sigma_x^2/2T, \quad K_y = \sigma_y^2/2T. \tag{1}$$

If the wind components $u(t)$, $v(t)$ at time t are also found, then using all the values from all the trajectories, ensemble means $\bar{u}$, $\bar{v}$ and variances $\overline{u'^2}$, $\overline{v'^2}$ may be readily be determined. In addition, the Lagrangian autocorrelation coefficients

$$R_u(\xi) = \overline{u'(t)\,u'(t+\xi)}/\overline{u'^2}, \quad R_v(\xi) = \overline{v'(t)\,v'(t+\xi)}/\overline{v'^2}, \tag{2}$$

for a series of lag times ξ can be calculated.

Using G. I. Taylor's equation in the form:

$$\sigma_x^2(T) = 2\overline{u'^2}\int_0^T\int_0^t R_u(\xi)\,\mathrm{d}\xi\,\mathrm{d}t, \tag{3}$$

we have for 'small' travel times when $R_u(\xi) \approx 1$

$$\sigma_x^2(T) \approx \overline{u'^2}T^2, \tag{4}$$

and for 'large' travel times when $R_u(\xi) \to 0$ and the area under the autocorrelogram tends to a constant value τ_u, the integral time scale,

$$\sigma_x^2(T) \approx 2\overline{u'^2}\tau_u T, \tag{5}$$

where $$\tau_u = \int_0^t R_u(\xi)\,\mathrm{d}\xi \quad \text{for large } t. \tag{6}$$

It would therefore be expected that for small times of travel σ_x^2 would be proportional to T^2 and as the largest eddies finally dominate the diffusion process that σ_x^2 would vary with T. Then from (1) and (5)

$$K_x = \overline{u'^2}\tau_u, \quad K_y = \overline{v'^2}\tau_v. \tag{7}$$

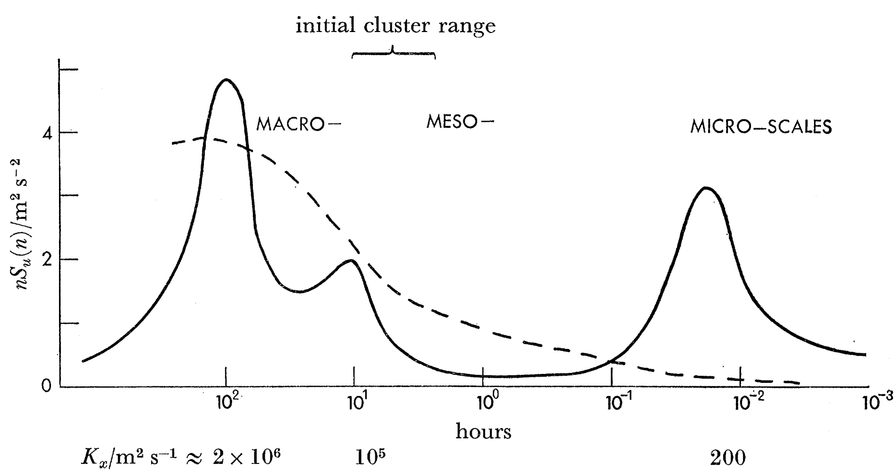

FIGURE 1. Examples of atmospheric energy spectrum determinations. ——, Van der Hoven's (1957) values near the surface; – – –, mean free atmosphere values from Pinus *et al.* (1967).

The determination of the large scale eddy diffusivities by this method depends on the form of the autocorrelograms and the rapidity with which $R(\xi)$ falls to small values. It requires a period of several days for the 'large' travel time conditions to be applicable and as it is very difficult to obtain accurate trajectories for this time this severely limits the method. It has been found that although the form of the autocorrelograms sometimes approximates to an exponential decay with time it more often varies in an oscillatory manner and a damped cosine curve for example would be more appropriate. The presence of negative autocorrelation values may lead to possible regions of contractions in spreading plumes of marked particles (Taylor 1921). This form of the autocorrelogram appears to be mainly due to the presence of well marked large scale waves and has also been observed in experiments in the friction layer, constant level balloon work and in simple spatial correlations. In order to estimate the integral time scales most authors (see, for example, Durst, Crossley & Davis 1959; Edinger & Rapp 1957; Kao 1962; Kao & Bullock 1964; Murgatroyd 1969*a*) have had to fit an analytical form to the autocorrelograms and hence extrapolate to infinite lag times. Values of horizontal eddy diffusivities obtained by this method will be representative of the largest scale eddies and have characteristic values of the order of $10^6\,\mathrm{m^2\,s^{-1}}$ (see figure 1), whereas those corresponding to the microscales (and excluded from this work by the assumption of constant winds in the chart intervals) are about 4 orders of magnitude smaller. Since the diffusivity varies greatly with the eddy size (roughly according to Richardson's (1926) four-thirds power law) values determined in any experiment will depend principally on the effective sample of eddy sizes which are encountered. In small scale or short period tests the larger eddies produce periodic oscillations of a plume or cluster resulting in dispersions or even contractions locally but these are not real diffusive effects. It should also be mentioned that in addition to the requirement that the experimental determination of the large scale diffusivities should be based on a full sample of all the atmospheric eddies including the largest there is an upper limit to the sampling time T of about 15 days in (1) imposed by the finite size of the atmosphere (see Angell & Hass 1966).

(*b*) *Constant level balloon experiments*

If a series of balloons are released from a given location and weighted to float on constant density surfaces their trajectories may be tracked and the dispersion of their end points at given times after release studied in the same way as those of the geostrophic trajectories. Investigations of diffusivity based on this technique (see, for example, Angell 1961; Kao 1965) may be used to define the probable areas in which balloons can be expected to be dispersed at different times. The data are basically more accurate than those from geostrophic trajectory calculations and may be obtained over longer periods but the objection that they do not take vertical motions into account still remains. This could result in large errors when the vertical wind shear is large.

(*c*) *Application to global transport and dispersion*

If a trace substance has a mass mixing ratio r with a mean value $\bar{r}$ and corresponding deviation r' such that

$$r = \bar{r} + r', \tag{8}$$

the continuity equation for this substance referred to Cartesian coordinates (x, y, z) with corresponding wind components (u, v, w), time t and air density ρ is

$$\rho\frac{\mathrm{d}\bar{r}}{\mathrm{d}t} + \frac{\partial}{\partial x}\rho\overline{r'u'} + \frac{\partial}{\partial y}\rho\overline{r'v'} + \frac{\partial}{\partial z}\rho\overline{r'w'} = S, \tag{9}$$

where S represents a source term. The transport of tracers on a global scale is often studied using (9) with the mean values referring to averages round latitude circles over a period of a month or season, thus confining the investigation to mean conditions on a height–latitude two-dimensional cross section. If the averages with respect to time are denoted by an overbar (with corresponding deviations by a prime) and those with respect to space by square brackets (9) then takes the form

$$\rho\left\{\frac{\partial[\bar{r}]}{\partial t} + [\bar{v}]\,\frac{\partial[\bar{r}]}{\partial y} + [\bar{w}]\frac{\partial[\bar{r}]}{\partial z}\right\} + \frac{\partial}{\partial y}\rho\{[\overline{r'v'}] + [\bar{r}^*\bar{v}^*]\} + \frac{\partial}{\partial z}\rho\{[\overline{r'w'}] + [\bar{r}^*\bar{w}^*]\} = S. \tag{10}$$

In (10) the first group of terms on the left hand side contains the contributions due to the components $[\bar{v}]$, $[\bar{w}]$ of the mean circulation. The other terms are due to the space averaged transient eddy fluxes $[\overline{r'v'}]$, $[\overline{r'w'}]$ and the standing eddy fluxes $[\bar{r}^*\bar{v}^*]$, $[\bar{r}^*\bar{w}^*]$. The asterisk denotes a deviation at one location of the time mean from the space–time mean round the latitude circle. The magnitudes of $[\bar{v}]$ and $[\bar{w}]$ are now fairly well known (see, for example, Vincent 1968; Murgatroyd 1969*b*). The values of the eddy fluxes are frequently combined and attempts made to express them in terms of a flux–gradient relation of the form

$$[\overline{r'v'}]+[\bar{r}^*\bar{v}^*] = -K_y\,\partial[\bar{r}]/\partial y, \tag{11}$$

where K_y is an eddy diffusion coefficient. This procedure, although mathematically convenient, is certainly not realistic as regards the standing eddies but it may be possible in some cases to neglect their contributions compared with those of the transient eddies. It has been observed also that for certain tracers, e.g. heat and momentum the application of (11) would lead to negative values of K_y, i.e. there is apparently counter-gradient transfer. A more realistic model still retaining the mixing length concept may be obtained by treating the eddy diffusivity as a tensor, writing

$$\left.\begin{aligned}[\overline{r'v'}] &= -\left(K_{yy}\frac{\partial[\bar{r}]}{\partial y}+K_{yz}\frac{\partial[\bar{r}]}{\partial z}\right),\\ [\overline{r'w'}] &= -\left(K_{zy}\frac{\partial[\bar{r}]}{\partial y}+K_{zz}\frac{\partial[\bar{r}]}{\partial z}\right),\end{aligned}\right\} \tag{12}$$

and Reed & German (1965) and Davidson, Friend & Seitz (1966), for example, have obtained more realistic models for the transport of radioactive tracers in the stratosphere using this approach. The form of (12) is consistent with the observation that the large scale meridional motion of air parcels usually takes place at an angle α ($\sim$ 1 mrad) to the horizontal and this angle is not the same as that of the isopleths of the mixing ratio to the horizontal. This is the mechanism of 'slant-wise' convection (Sheppard 1963) for heat transfer. The estimation of values of K_{yy}, K_{zz} and $K_{yz} \approx K_{zy}$ on a global basis can only be tentative at present. Taking $K_{yy} \propto [\overline{v'^2}]$ at each latitude, i.e. assuming the integral time scale at a given height is sensibly invariant with latitude and using the values of K_{yy} estimated by Murgatroyd (1969*a*) from geostrophic trajectory studies for 55° N, the values of K_{yy} scaled to other latitudes are given in table 1*a*. It may also be shown that

$$K_{yz} \approx [\bar{\alpha}]\,K_{yy}, \tag{13}$$

$$K_{zz} \approx ([\bar{\alpha}]^2+[\overline{\alpha'^2}])\,K_{yy}. \tag{14}$$

The direct determination of values of $[\bar{\alpha}]$ requires the accumulation of statistics of w and v, the former of which is difficult to determine accurately. Another possible method is to obtain independent estimates of $[\overline{r'v'}]$ in (12) and use these to determine K_{yz} and hence $[\bar{\alpha}]$ from (13). This method was employed by Reed & German (1965) using global heat flux data (global data do not exist for any inert tracer). A similar set of estimates of K_{yz} and $[\bar{\alpha}]$ using the values of K_{yy} in table 1*a* is given in tables 1*b* and *c*. Minimum limits of K_{zz} are set by $[\bar{\alpha}]^2K_{yy}$ but there are no independent estimations of $[\overline{\alpha'^2}]$ and its variation with latitude at present available. Table 1 indicates that K_{yy} is always positive and is a maximum in the upper troposphere and at mid-latitudes. K_{yz} is three orders smaller than K_{yy} and is positive in the troposphere and negative in the lower stratosphere. K_{zz} is always positive and about six orders less than K_{yy}.

Although the formulation above has been applied with some success to global tracer dispersion studies it has several major weaknesses. For more detailed work three-dimensional numerical forecast models, which will give data on vertical motions and also avoid some of the difficult

Table 1. Estimated mean latitudinal values of K_{yy}, K_{yz} and $[\overline{\alpha}]$ (see equation (13))

	summer								winter								
latitude/deg	80	70	60	50	40	30	20	10	10	20	30	40	50	60	70	80	mean $10^{-4}\ \tau$/s
mbar								(a) $10^{-6}\ K_{yy}$/m^2 s^{-1}									
30	0.4	0.4	0.5	0.8	0.8	0.5	0.5	0.7	0.5	0.7	0.9	1.7	3.1	3.4	3.4	3.6	4.3
50	0.7	0.9	0.8	1.0	1.0	0.7	0.6	0.6	0.9	0.9	1.2	1.6	2.5	3.0	3.6	3.9	5.0
100	0.6	0.8	1.1	1.7	1.7	1.1	0.9	0.8	1.5	1.9	2.6	2.8	2.7	3.1	2.8	2.2	3.4
200	1.0	1.5	2.2	3.2	2.7	1.5	0.9	0.6	1.2	2.3	3.8	4.1	3.4	3.0	2.1	1.5	1.8
300	1.9	2.1	2.9	3.0	2.0	0.9	0.4	0.3	0.8	1.6	3.1	4.1	4.2	3.6	2.4	1.8	1.7
500	1.3	1.3	1.6	1.6	1.0	0.6	0.3	0.2	0.4	0.9	1.7	2.5	2.9	2.5	1.9	1.5	1.9
700	1.8	2.2	2.7	2.9	1.8	1.3	0.9	0.7	0.8	1.4	2.7	3.8	4.8	4.3	3.3	2.6	5.6
								(b) $10^{-3}\ K_{yz}$/m^2 s^{-1}									
30		0	−0.1	−0.4	−0.3	−0.2	−0.2	−0.2	−0.1	−0.5	−0.3	−0.5	0.1	1.2	1.1		
50		−0.1	−0.3	−0.6	−0.6	−0.4	−0.3	−0.2	−0.2	−0.4	−0.8	−1.0	−0.7	0.8	2.0		
100		−0.1	−0.7	−1.4	−1.4	−0.8	−0.5	−0.3	−0.4	−1.0	−2.3	−2.5	−1.5	0.7	1.6		
200		−0.7	−1.1	−1.5	−1.4	−0.9	0.6	0.5	1.5	2.0	0.6	−1.5	−1.3	−0.5	0.2		
300		−0.6	0.7	2.9	1.5	−0.1	0.5	0.7	1.1	1.6	3.7	4.5	3.1	1.6	0.9		
500		−0.7	0.2	0.4	−0.1	0.5	0.2	0.1	0.5	1.1	2.7	3.5	2.3	1.2	−0.2		
700		0.8	0.7	1.3	0.7	0.5	0.3	0	0.3	0.8	1.7	3.6	3.2	1.1	0.3		
								(c) $10^3\ [\overline{\alpha}]$/rad									
30		−0.1	−0.3	−0.5	−0.4	−0.4	−0.3	−0.3	−0.1	−0.2	−0.4	−0.3	0	0.4	0.3		
50		−0.1	−0.4	−0.6	−0.6	−0.5	−0.5	−0.3	−0.3	−0.5	−0.7	−0.6	−0.3	−0.3	0.6		
100		−0.1	−0.7	−0.8	−0.9	−0.7	−0.6	−0.4	−0.3	−0.5	−0.9	−0.9	−0.5	0.2	0.6		
200		−0.5	−0.5	−0.5	−0.5	−0.6	0.7	0.7	1.3	0.9	0.1	−0.3	−0.4	−0.2	0.1		
300		−0.3	0.3	1.0	0.7	−0.1	1.1	2.5	1.4	1.0	0.8	0.9	0.7	0.4	0.4		
500		−0.5	0.1	0.3	−0.1	0.9	0.8	0.7	1.3	1.3	1.6	1.4	0.8	0.5	−0.1		
700		0.3	0.3	0.4	0.4	0.4	0.3	0.1	0.5	0.5	0.7	0.9	0.7	0.3	0.1		

problems introduced by the averaging processes, will be required. Considerable progress in their use for these studies is already evident, for example in the results given by Smagorinsky, Manabe & Holloway (1965), Manabe, Smagorinsky & Stickler (1965), and Manabe & Hunt (1968).

Studies of cluster dispersion

(a) *Large data samples*

The analogous equation to (3) for mean square separation $\overline{x_r^2}$ at time T of pairs of particles having a relative velocity $u_r(t)$ and an initial separation x_{r_0} is (Batchelor 1950):

$$\overline{x_r^2} = \overline{x_{r_0}^2} + 2\int_0^T \int_0^t \overline{u_r(t)\, u_r(t+\xi)}\, \mathrm{d}\xi\, \mathrm{d}t. \tag{15}$$

At small separations u_r will be determined by the small scales of motion but at greater distances the larger scales will become progressively more important. When T is small (15) reduces to

$$\overline{x_r^2} \approx \overline{x_{r_0}^2} + \overline{u_r^2}\, T^2. \tag{16a}$$

Similarity theory for homogeneous turbulence predicts that for this case

$$\overline{x_r^2} \propto [\mathrm{constant} + (\epsilon x_{r_0})^{\frac{2}{3}} T^2], \tag{16b}$$

and

$$\overline{x_r^2} \propto \epsilon T^3, \tag{17}$$

at 'intermediate' times when the distance apart of the particles has become independent of their initial separation. ϵ is the rate of dissipation of eddy kinetic energy. For very long travel times it may be shown (see, for example, Pasquill 1962, p. 104) that the mean square separation of a pair of particles tends to twice the mean square separation of particles released in sequence from a fixed position. Good agreement with (16*a*) and (17) has been found by Gifford (1957*a*, *b*) for (microscale) studies of the rates of spread of smoke puffs.

The study of cluster dispersion by the large scale eddies using trajectories computed from charts of wind fields or possibly constant level balloon experiments is more complex than the continuous point source work. The behaviour of the cluster is strongly dependent on its size in relation to the eddy sizes. Eddies much larger than the cluster size will simply transport it as a whole, eddies much smaller will cause diffusion while those of comparable size will primarily result in deformation due to the wind shear across the cluster. As it expands it experiences the effect of all the different scales and usually spreads into a long thin band elongated in the direction of the mean motion and which sometimes folds back on itself (see, for example, Welander 1955; Mesinger & Milovanovic 1963). Geostrophic trajectories were used by Durst & Davis (1957) to study the variation with time up to 36 h of the separation of particles initially spaced from 80 to 560 km apart and they found the separation distance to be proportional to the first power of the time and to the 0.86 power of the initial separation distance (cf. 16*a*, 16*b*). Mesinger & Milovanovic (1963) used a simplified 500 mbar (50 kN m^{-2}) single level numerical forecast model which gave 8-day integrations for the hemisphere and adapted it to work out the two-dimensional trajectories of particles initially at the grid points about 400 km apart. They found that the rates of spread of the clusters formed by different combinations of the data from the various trajectories were in agreement with (16*a*) up to times of several days. However, when they were compared with (17) the exponent of T never exceeded 1.6 and it seemed clear that it would never reach the predicted value of 3 since at very long times the clusters would be expected to behave in a similar manner to plumes, i.e. with an exponent of unity in this equation. They also found the zonal expansion rates to be more than an order greater than those meridionally. Angell & Hass (1966) found that with particles having a very large initial separation, 1–2 Mm, the separation distance increased as about the 0.6 power of the time for the first ten days of travel but thereafter it stabilized at a value of about 6.4 Mm. Their experiment and also that of Mesinger (1965) used electronic computations of two-dimensional diagnostic trajectories from a hemispherical grid of points to investigate the probable behaviour of a global observing network formed by a large number of constant level balloons. It appears that whereas the macroturbulence tends within 10 to 15 days to produce a random distribution of initially regularly spaced particles through the non-divergent part of the wind flow, the divergent component produces departures and these can be studied in terms of distance–neighbour or areal concentration statistics. The results so far available suggest that the effects of concentrating or dispersing the particles in particular areas is not likely to be serious enough to invalidate the system as a global observing network. The affected areas will depend principally on the mean circulation and standing eddies with concentrations tending to occur in upper level ridges in the flow pattern usually on the western sides of the continents and in areas of weak pressure gradient.

(*b*) *Individual case studies*

The object of the studies discussed above has been to predict the average behaviour of large data samples for planning or climatological purposes but the behaviour of a large individual cluster in a given location and synoptic situation will generally require separate consideration.

The displacement and development of a two-dimensional sheet in terms of its translation, contraction or expansion (divergence), rotation (vorticity) and deformation (stretching and shearing) has been discussed by Petterssen (1956, p. 32 *et seq.*). Distortion of the shape of the cluster and large changes in the separation of its component particles due to the deformation terms take place before they diffuse into the surroundings. Vertical motions will add considerably to this process by moving particles into regions of different horizontal wind components when vertical shear is present. In this section, however, only two-dimensional deformation will be considered following Djuric (1964, 1966).

In an area which is sufficiently small for the motion field to be regarded as linear

$$u = \tfrac{1}{2}Bx, \tag{18}$$

$$v = -\tfrac{1}{2}By, \tag{19}$$

where

$$B = \frac{\partial u}{\partial x} - \frac{\partial v}{\partial y}. \tag{20}$$

Here the (x, y) axes are rotated so that B is the modulus of the deformation and an initially square cluster is deformed into a rectangle by dilatation along its x axis and contraction along its y axis. In a two-dimensional non-divergent field $B = 2\partial u/\partial x$ and the area A of the cluster remains unchanged. The variance σ^2 of the position of all its particles about its centre of gravity, however, will increase. In the case of an ellipse

$$\frac{x^2}{a^2} + \frac{y^2}{b^2} = 1,$$

which would be formed by the deformation of a circle

$$\sigma^2 = \frac{1}{A}\iint_A (x^2 + y^2)\,\mathrm{d}x\,\mathrm{d}y = \tfrac{1}{4}(a^2 + b^2). \tag{21}$$

The rate of extension of the major axis is given by

$$\frac{\mathrm{d}a}{\mathrm{d}t} = a\frac{\partial u}{\partial x} = \tfrac{1}{2}aB,$$

so that
$$a = a_0 \exp\left(\tfrac{1}{2}Bt\right), \tag{22}$$

$$b = a_0 \exp\left(-\tfrac{1}{2}Bt\right), \tag{23}$$

and
$$\sigma^2 = \sigma_0^2 \cosh Bt = \sigma_0^2\left(1+\frac{B^2t^2}{2!}+\frac{B^4t^4}{4!}+\ldots\right). \tag{24}$$

Equation (24) indicates that the variance of the cluster points about the centre of gravity to a first approximation will vary with the time squared and the initial cluster size and Djuric's treatment of the effect of deformation in curved shear flow leads to the same conclusion. This kind of variation would be expected using (16) but the effects of diffusion which involve areal increases and those of deformation which only involve changes of shape are quite different. When combined, e.g. with different deformation at different levels and diffusion between levels, the rate of disperson of a three-dimensional cluster is likely to be considerably increased.

In the following section a preliminary case study of large scale dispersion in a given synoptic situation using a numerical forecast integration will be described. The results of the latter are used in investigations both of the spread of trajectories from continuous point sources and of the dispersion of large scale clusters with particular reference to the effects of the deformation fields.

A pilot study using the Meteorological Office's 10 level numerical model

(a) *Method*

The Meteorological Office's numerical forecast model developed by Bushby & Timpson (1967) has 10 levels spaced at 100 mbar pressure intervals from the surface to the 100 mbar level and uses the primitive equations to provide forecasts over 24 to 48 h for an area covering most of the eastern Atlantic and western Europe. The basic grid lengths are approximately 100 km, the time step for integration 100 s and the model includes a reasonable representation of most of the major small scale phenomena and physical processes in the troposphere, i.e. condensation, evaporation, subgrid scale convection, surface topography and lateral diffusion. As the integration proceeds the values at 45 min intervals of the three 'wind' components u, v and ω $(= \mathrm{d}p/\mathrm{d}t)$ over the area and at the different pressure levels are stored on magnetic tape as part of the main prediction programme. A supplementary programme was used to step forward in each of these intervals the position of any given particle using these stored wind values and linearly interpolating the wind in space between the values at the grid points. Hence by specifying given starting points sequential trajectories through these points could be constructed at 45 min intervals to simulate continuous sources. Alternatively by specifying combinations of different starting points to define clusters at an initial time the trajectory through each point could be determined and hence the evolution of the cluster. In addition to the three dimensional trajectories the effect of excluding contributions by the vertical wind components was investigated by finding similarly the trajectories of particles confined to given pressure surfaces using only the horizontal wind components. Supplementary data included the mean wind components in each interval for use if required to construct Lagrangian autocorrelograms and also a print-out of Eulerian data at fixed points.

(*b*) *The synoptic situation and the kinematics of the horizontal wind field*

The period chosen was the last 18 h of a 24 h integration starting at 00.00 G.M.T. on 1 December 1961. During that day a small wave depression with central pressure of 1000 mbar moved ENE along a well marked frontal boundary from about 50° N 23° W to 53° N 5° E and deepened to 987 mbar. Considerable rain fell over southern England and the movement of the depression,

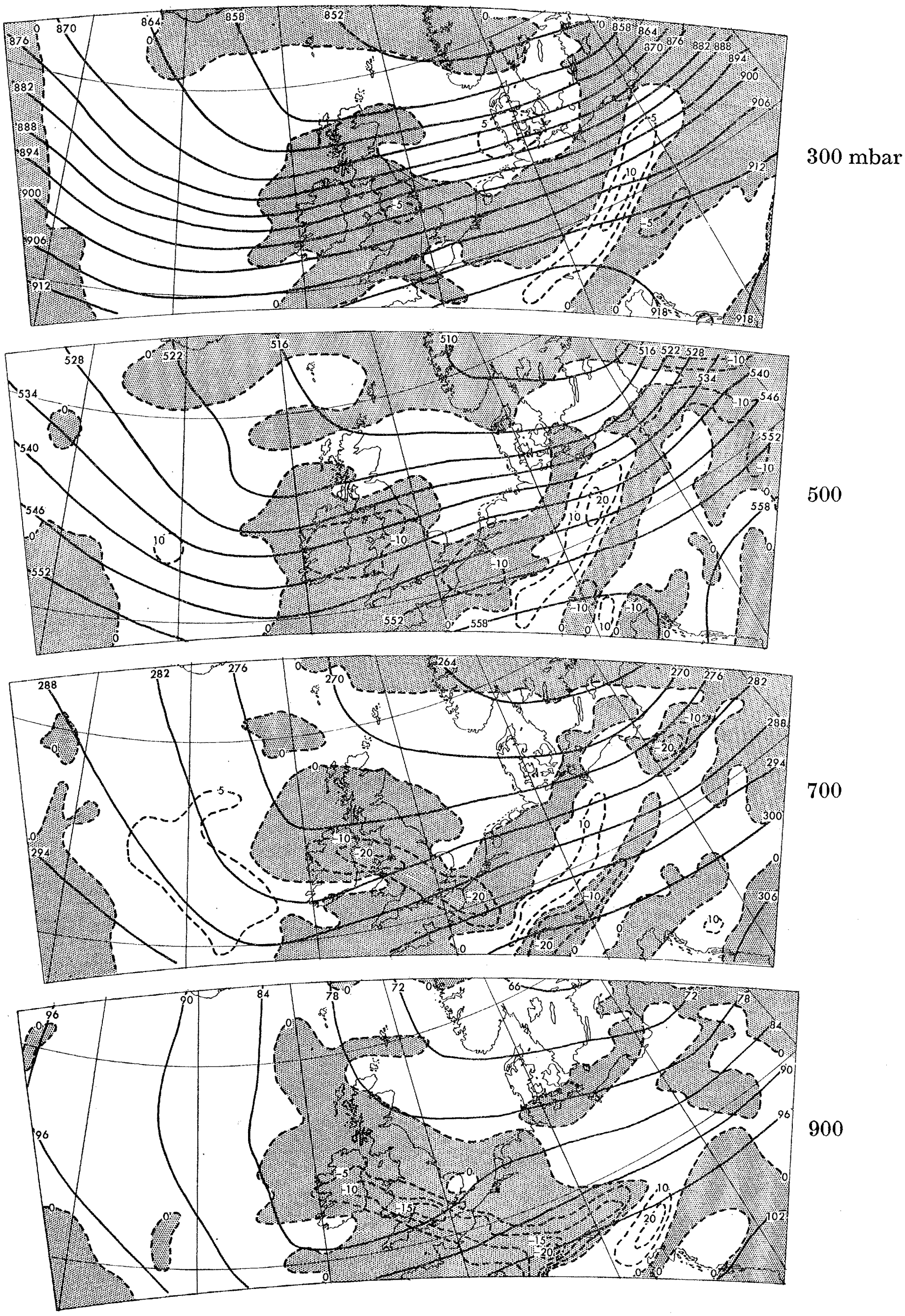

FIGURE 2. Full lines forecasted contour charts at 12.00 G.M.T. on 1 December 1961 at the 900, 700, 500 and 300 mbar levels at intervals of 60 m. Dashed lines isopleths of vertical motion in millibars per hour with upwards motion stippled.

the frontal positions and the rainfall amounts were forecasted well by the model (see Bushby & Timpson 1967 for further details). There was also a larger area of low pressure to the northeast of Scotland and this moved ENE during the period with another small centre forming over Scotland and moving quickly east. The surface winds were generally NW to N to the west of these low pressure areas and WSW to the east.

The upper wind fields depicted by the forecasted contour fields and vertical velocities in millibars per hour at 12.00 h G.M.T. on 1 December 1961 are shown in figure 2. The progressive

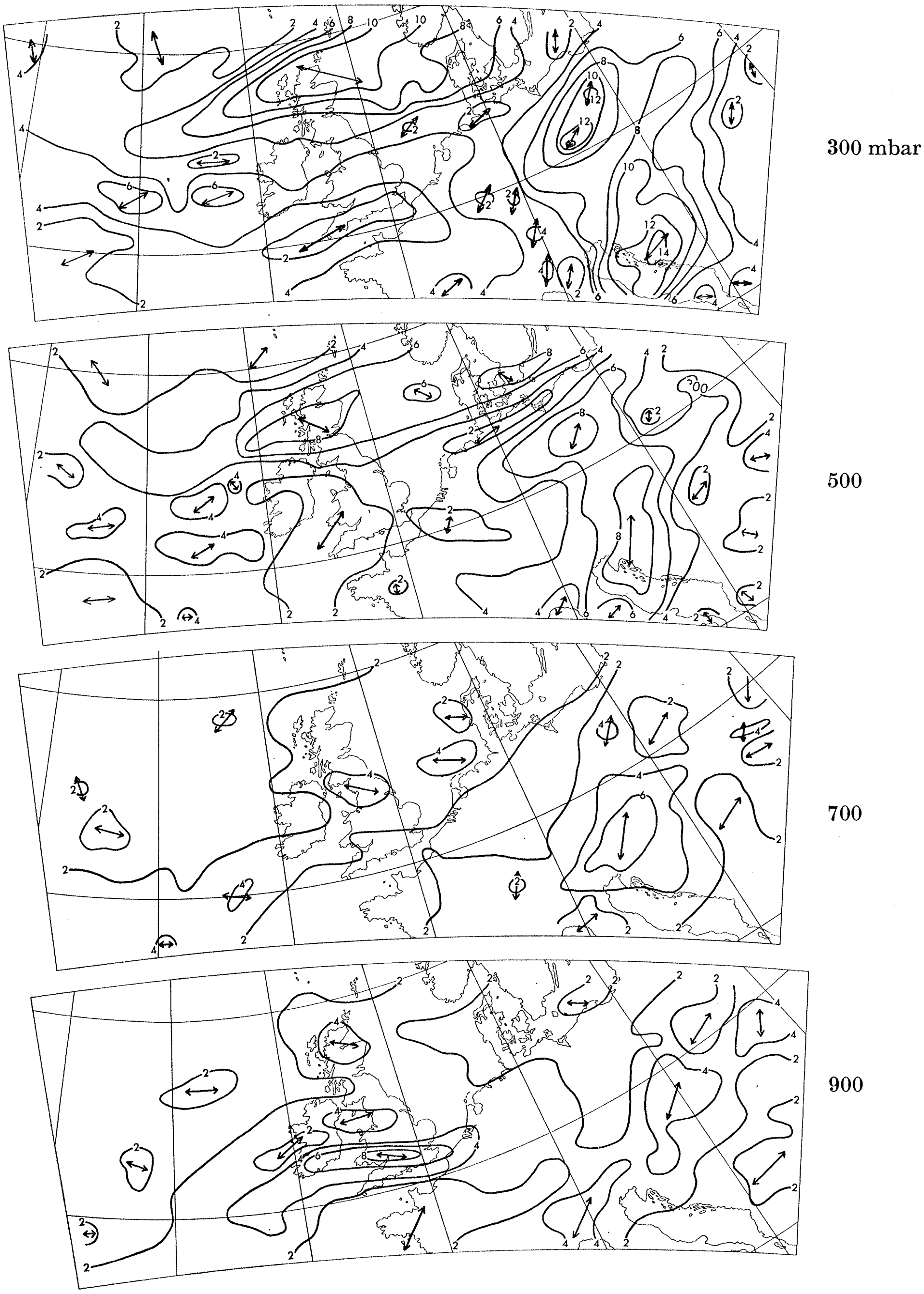

FIGURE 3. Corresponding isopleths of deformation in $10^{-5}\,s^{-1}$.
Full lines with arrows indicate the axis of stretching.

PHILOSOPHICAL TRANSACTIONS OF THE ROYAL SOCIETY A MATHEMATICAL, PHYSICAL & ENGINEERING SCIENCES

change with height from the lower tropospheric winds to the strong westerly winds at the 300 mbar level blowing round the south of an upper trough, which also moved steadily eastwards during the period, is the most noteworthy feature. The accompanying vertical wind field appears to have considerably more smaller scale variation than that of the horizontal components. Its predominant feature is the upwards motion at all levels over the southern part of the British Isles with a corresponding region of subsidence over the eastern Atlantic.

The divergence and vorticity fields for these levels were calculated over 200 km grid squares but are not reproduced here. At 900 mbar there was a large area of convergence with maximum values about $3 \times 10^{-5}\,s^{-1}$ over and near the west of the British Isles with areas of divergence further west. These areas were generally surmounted at the 500 and 300 mbar levels by regions of the opposite sign. Further east over the continent there were alternately regions of divergence

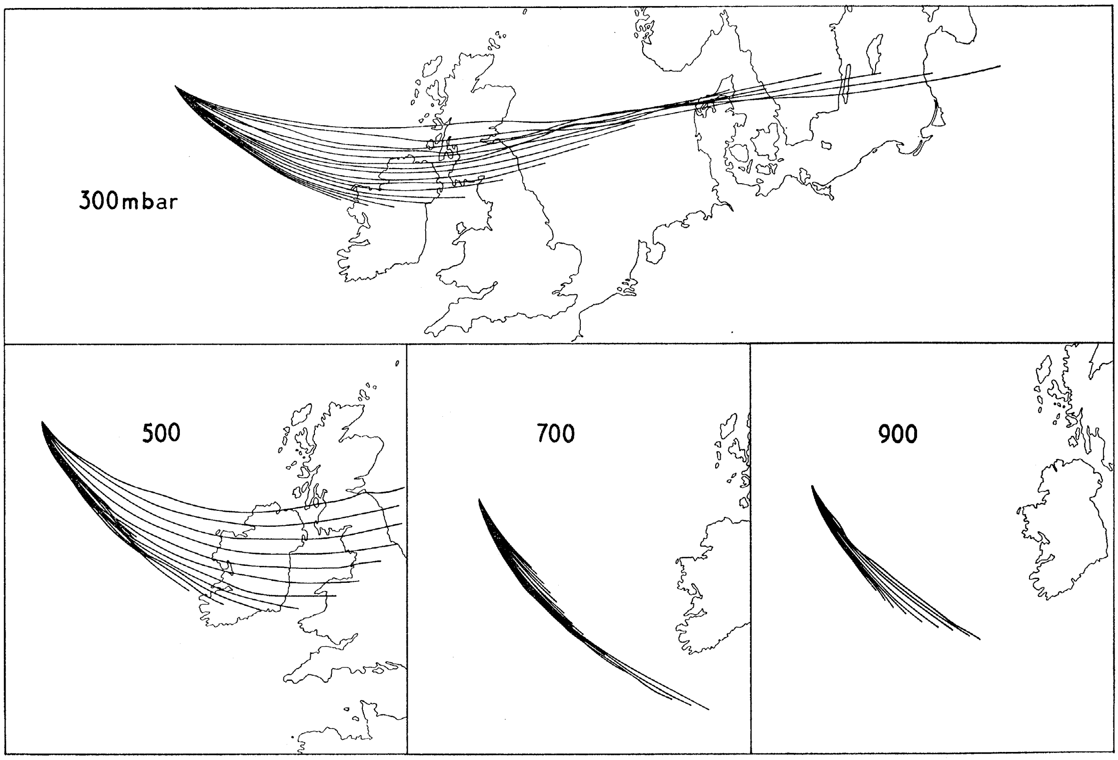

FIGURE 4. A selection of sequential horizontal trajectories through given points at the 300, 500, 700 and 900 mbar pressure levels obtained from the Bushby–Timpson model integrations for 1 December 1961.

and convergence with considerable smaller scale detail. Over most of the charts the divergence values were within $\pm 2 \times 10^{-5}\,s^{-1}$ but in small areas occasionally reached $\pm 4 \times 10^{-5}\,s^{-1}$.

The dominant feature of the vorticity field at the 900 mbar level was a large area of positive (cyclonic) vorticity with a central value of $10 \times 10^{-5}\,s^{-1}$ centred over the southern Irish Sea. A similar centre somewhat further to the northwest was evident at the higher levels, with a value of $12 \times 10^{-5}\,s^{-1}$ at about 57° N 10° W at the 300 mbar level. Regions of negative vorticity of about $4 \times 10^{-5}\,s^{-1}$ were found over southern Europe at the 900 mbar level. At the higher levels the vorticity was negative over the southern British Isles and western Europe and positive over the northern British Isles and Scandinavia in the upper trough. At the 300 mbar level values reached 10 to $12 \times 10^{-5}\,s^{-1}$.

The corresponding deformation field is shown in figure 3. The general direction of the dilatation axes in the areas of maximum or minimum deformation are also indicated. There again appears to be considerable detail and apparently small scale variations. As with the vorticity values, the magnitudes are generally several times those of the divergence (a necessary condition for (24) to be applicable) and reach 4 to $8 \times 10^{-5}\,\mathrm{s}^{-1}$ at the lower levels increasing to 10 to $14 \times 10^{-5}\,\mathrm{s}^{-1}$ at the 300 mbar level. The directions of the stretching axes are mainly zonal over the eastern Atlantic and the British Isles and meridional over western Europe. There is a well marked maximum of deformation with zonal stretching at the 900 mbar level over the British Isles in the region of the main frontal zone. Figure 3 refers only of course to one time, 12.00 h G.M.T. whereas the distortion of a cluster will take place in a deformation field which varies with time. However, if the dispersion σ^2 of a cluster is measured over the forecast period it would be expected that the value of B calculated from (24) would agree approximately with the general magnitudes for the areas under consideration in figure 3.

(c) *Results of the continuous point source computations*

Figure 4 shows a plot of sets of constant pressure level trajectories through a given fixed point at 300, 500, 700 and 900 mbar. The effects of the stronger wind speeds at the 300 mbar level and the larger meridional variability at 300 and 500 mbar are well marked. Owing to the limited time of the forecast the trajectories starting at the earlier times are continued for longer periods

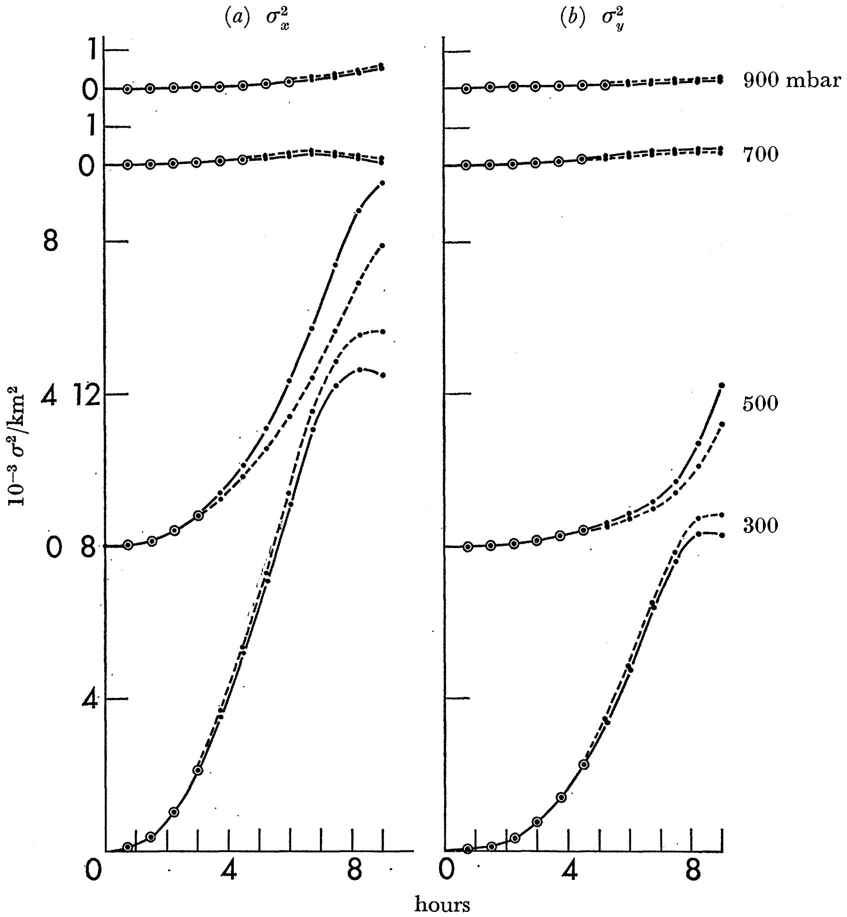

FIGURE 5. Horizontal variances (a) σ_x^2, (b) σ_y^2 of the end points of the trajectory sets shown in figure 4 plotted for the first 9 h of travel. ——, Trajectories confined to the given pressure levels; – – – –, three dimensional trajectories.

than those starting later so that a full comparison of all the trajectories is only possible for a 9 h period after the passage through the fixed point. Plots of the variances against time are shown in figure 5 for both the three-dimensional and constant pressure level sets and a comparison of the

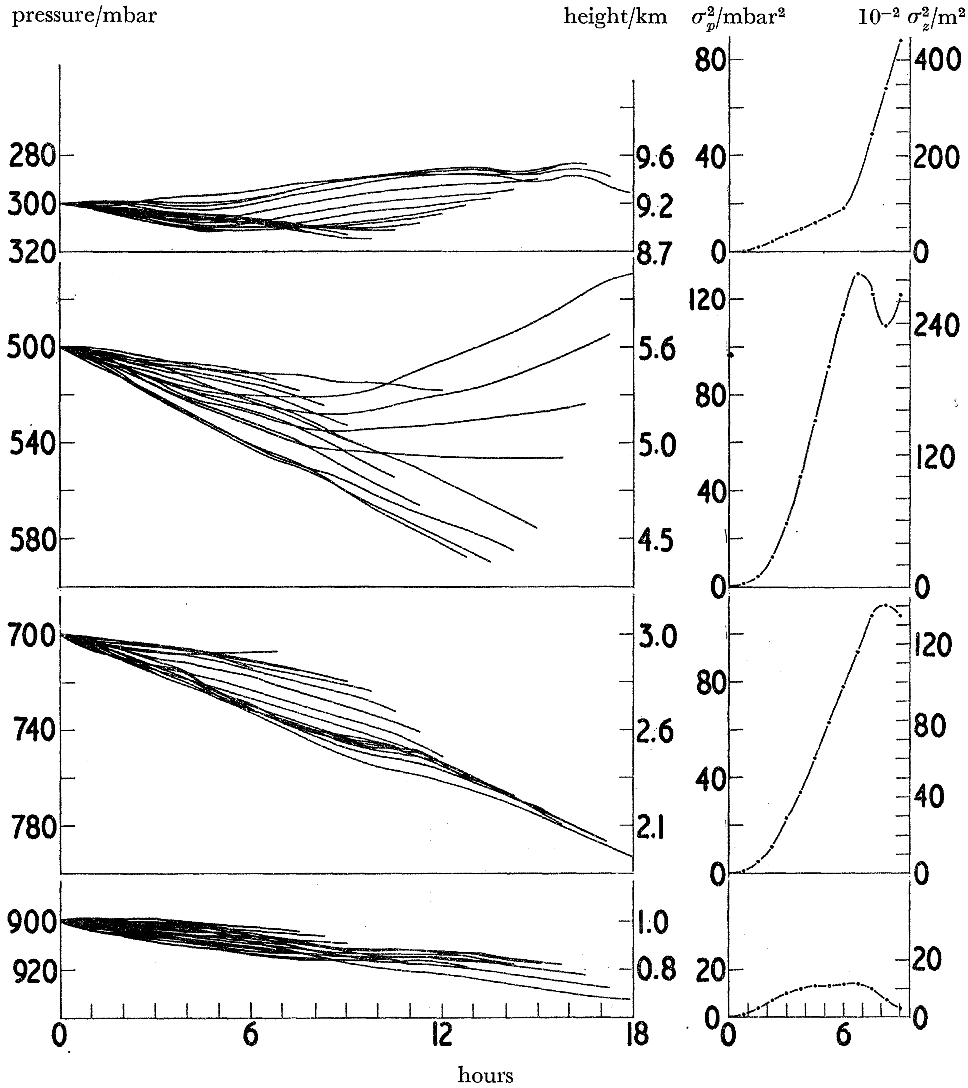

FIGURE 6. The vertical displacements of the three dimensional trajectory points plotted against time. The right hand graphs show the corresponding changes of the variances σ_p^2, σ_z^2 with time.

variances in the two cases shows that for this example at least the use of constant level data only would not have produced serious errors, i.e. 10 to 20 % at the most in estimates of the horizontal variances. This conclusion may not, however, be valid in other examples where the vertical wind shear is greater.

Figure 6 shows the corresponding trajectories and the variances of their end-points in the vertical plane for the three-dimensional sets. σ_x^2, σ_y^2 and σ_z^2 for the three-dimensional sets of trajectories and also the values of β at each point calculated from equations of the type

$$\sigma_x^2 = kt^\beta, \tag{25}$$

where k is a constant are listed in table 2. When the exponent $\beta = 2$ this equation should

TABLE 2. SUMMARY OF DISPERSION DATA σ_x^2, σ_y^2, σ_z^2 AND CORRESPONDING EXPONENTS OF RATES OF SPREAD (SEE EQUATION (25)) FOR CONTINUOUS POINT SOURCE EXPERIMENT

time/h ...	1	2	3	4	5	6	7	8	9	10	11	12
						900 mbar						
$10^{-7}\,\sigma_x^2/\mathrm{m}^2$	1	2	3	5	7	10	14	20	28	36	47	60
$10^{-7}\,\sigma_y^2/\mathrm{m}^2$	0	2	3	4	6	7	9	12	17	19	21	22
$10^{-3}\,\sigma_z^2/\mathrm{m}^2$	0.08	0.33	0.58	0.83	1.00	1.08	1.08	1.17	1.17	1.08	0.58	0.33
β_x		1.0	1.5	1.6	1.8	2.1	2.5	2.8	2.6	2.6	2.8	2.8
β_y		1.5	1.0	1.5	1.3	1.3	1.9	2.7	1.8	1.1	0.8	0.5
β_z		1.5	1.3	1.0	0.6	0.2	0.3	0.3	−0.6	−2.9	−6.3	−6.0
						700 mbar						
$10^{-7}\,\sigma_x^2/\mathrm{m}^2$	0	1	3	6	10	15	22	28	34	30	24	18
$10^{-7}\,\sigma_y^2/\mathrm{m}^2$	0	2	3	6	10	14	19	24	30	32	33	32
$10^{-3}\,\sigma_z^2/\mathrm{m}^2$	0.13	0.63	1.40	2.92	4.32	6.10	8.00	9.91	11.81	13.72	14.23	13.72
β_x		3.0	2.5	2.3	2.3	2.4	2.1	1.7	0.3	−1.7	−2.7	−4.0
β_y		1.5	2.0	2.3	2.0	1.9	1.8	1.8	1.2	0.5	0	−0.2
β_z		2.0	2.5	2.0	1.8	1.8	1.7	1.5	1.4	0.9	0	−2.1
						500 mbar						
$10^{-7}\,\sigma_x^2/\mathrm{m}^2$	4	18	43	79	126	185	259	346	441	566	692	787
$10^{-7}\,\sigma_y^2/\mathrm{m}^2$	1	4	9	18	29	42	58	77	103	144	215	326
$10^{-3}\,\sigma_z^2/\mathrm{m}^2$	0.22	0.87	2.60	5.64	9.98	14.97	19.96	24.73	28.42	26.47	23.65	26.47
β_x		2.2	2.2	2.1	2.1	2.1	2.2	2.1	2.2	2.2	1.7	1.1
β_y		2.0	2.3	2.2	2.1	2.1	2.1	2.3	2.9	3.9	3.7	4.9
β_z		2.7	2.7	2.6	2.3	2.0	1.7	1.4	0.3	−0.9	0	3.2
						300 mbar						
$10^{-7}\,\sigma_x^2/\mathrm{m}^2$	8	40	108	217	369	537	733	941	1155	1286	1355	1361
$10^{-7}\,\sigma_y^2/\mathrm{m}^2$	3	15	39	81	144	231	345	487	656	791	874	884
$10^{-3}\,\sigma_z^2/\mathrm{m}^2$	0	0.94	1.99	3.48	4.47	5.97	7.46	8.95	16.91	24.37	33.81	43.76
β_x		2.5	2.5	2.4	2.2	2.0	1.9	1.8	1.3	0.8	0.3	−0.2
β_y		2.4	2.5	2.6	2.6	2.6	2.6	2.5	2.1	1.4	0.6	−0.7
β_z		2.0	1.9	1.4	1.4	1.5	1.4	4.2	4.1	3.5	3.1	1.7

correspond to the 'small time' case of (4) and when $\beta = 1$ to the 'large time' case of (5). The results for the small data sample here, although very variable, give $\beta \approx 2$ for most of the period. Previous authors have noted that for these large scale motions several days of travel are required to reach the 'large time' diffusion condition and also that at shorter times the regular periodic motions due to the larger scale systems will cause variations in σ_x^2, σ_y^2 and σ_z^2 which cannot be ascribed simply to diffusion effects. Table 2 indicates also that σ_x^2 and σ_y^2 are of the same order with the former mainly being the larger by a small factor. σ_z^2 is 4 orders smaller at the 700 mbar level and 5 to 6 orders smaller at the other levels. The ratios of the diffusivities would be expected to be of the same general magnitude.

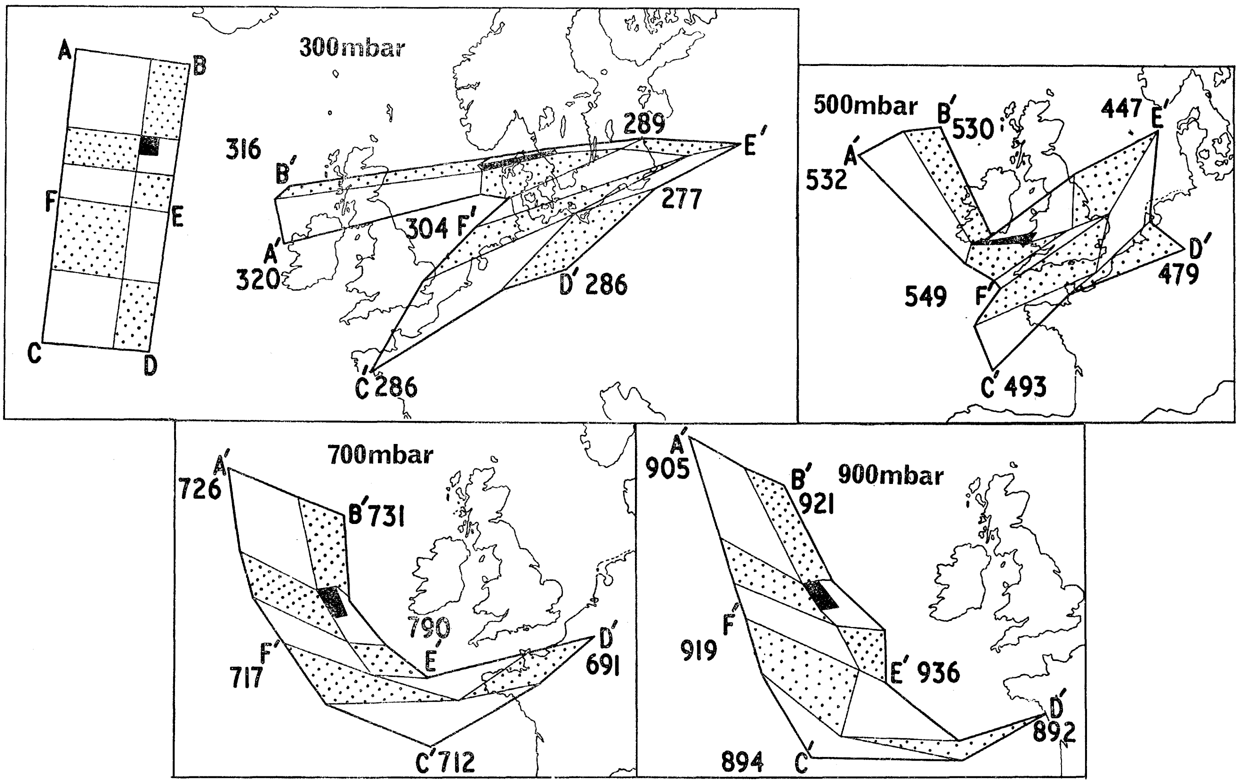

Figure 7. The development of clusters initially of the form ABCDEF at each level to clusters A′ B′ C′ D′ E′ F′ 18 h later. The final pressure levels of the different points on the clusters in millibars are also shown. Shaded and stippled areas show how the smaller clusters within the large area developed with time.

(d) *Results from the cluster computations*

Figure 7 shows how a selection of the clusters developed over a period of 18 h at each of the pressure levels 300, 500, 700 and 900 mbar. ABCDEF on the 300 mbar diagram defines the initial points and smaller clusters formed by internal grid points are marked by plain, stippled and shaded areas. The sizes examined included clusters of initial sizes of about 100 km (the small shaded square) up to 1600 km (initially a square of side AC). In each case A′ B′ C′ D′ E′ F′ defines the trajectory end points and their final pressure levels. The rapid distortion of each initial cluster is evident and it can be seen that the northernmost points AB were always in descending currents and the southeasterly point D in an ascending part of the airstream. At 300 mbar there was evidently a strong jet stream through the centre EF of the cluster whereas at lower levels most of the air was moving round the southwesterly section of a depression.

PHILOSOPHICAL TRANSACTIONS OF THE ROYAL SOCIETY A MATHEMATICAL, PHYSICAL & ENGINEERING SCIENCES

TABLE 3. SUMMARY OF DISPERSION DATA FOR THE CLUSTER EXPERIMENT σ_x^2, σ_y^2, σ_p^2

approx. initial cluster side/km		900 mbar							700 mbar						500 mbar						300 mbar					
	time/h ...	0	3	6	9	12	15	17¼	3	6	9	12	15	17¼	3	6	9	12	15	17¼	3	6	9	12	15	17¼
100	$10^{-8}\sigma_x^2/m^2$	37	36	39	43	46	51	60	31	29	29	31	35	27	29	45	112	197	307	349	38	115	227	332	474	593
	$10^{-8}\sigma_y^2/m^2$	34	36	36	39	44	47	50	39	41	45	50	54	129	41	45	33	15	6	13	34	13	11	24	13	3
	$\sigma_p^2/mbar^2$	0	2	3	11	12	15	14	3	9	30	34	29	36	1	41	49	40	33	48	2	3	43	56	39	36
200	$10^{-8}\sigma_x^2/m^2$	148	140	152	177	206	253	308	132	120	132	156	189	212	153	288	521	739	845	820	157	439	781	1174	1712	2292
	$10^{-8}\sigma_y^2/m^2$	133	138	139	145	152	157	164	146	167	178	189	203	216	126	96	60	73	180	318	115	44	38	32	10	37
	$\sigma_p^2/mbar^2$	0	6	4	8	5	3	10	3	15	38	26	67	102	11	91	266	667	1611	2845	6	31	141	117	72	50
400	$10^{-8}\sigma_x^2/m^2$	645	552	493	494	538	583	628	574	517	491	498	526	559	444	327	282	351	563	824	438	482	915	1826	3010	4076
	$10^{-8}\sigma_y^2/m^2$	544	593	636	673	730	807	861	578	613	640	664	681	686	664	798	938	1024	1045	1025	640	640	488	232	146	239
	$\sigma_p^2/mbar^2$	0	1	5	42	56	49	62	12	45	176	240	270	393	18	66	284	595	1166	1732	2	17	36	18	17	59
600	$10^{-8}\sigma_x^2/m^2$	1409	1353	1302	1383	1530	1723	1933	1308	1232	1245	1333	1456	1558	1265	1298	1460	1772	2147	2339	1306	1819	2946	4729	7085	9381
	$10^{-8}\sigma_y^2/m^2$	1211	1255	1306	1350	1424	1526	1600	1269	1321	1369	1434	1498	1531	1315	1363	1346	1267	1157	1117	1107	914	669	418	255	223
	$\sigma_p^2/mbar^2$	0	8	10	28	41	65	86	6	71	235	300	564	865	12	54	118	291	665	1065	11	38	130	170	153	197
800	$10^{-8}\sigma_x^2/m^2$	2434	2328	2251	2258	2312	2426	2571	2438	2118	2112	2800	3142	3491	2633	3114	3951	5358	7406	9267	2781	4049	6319	9893	14141	—
	$10^{-8}\sigma_y^2/m^2$	2123	2225	2327	2466	2690	2974	3157	2135	2471	2529	2088	2038	1980	1948	1757	1687	1683	1585	1551	1707	1337	1033	721	461	—
	$\sigma_p^2/mbar^2$	0	10	25	76	158	214	282	4	8	39	128	363	604	127	582	1425	1553	1049	1117	13	41	64	21	10	—
1200	$10^{-8}\sigma_x^2/m^2$	5204	5758	6651	7721	8981	10289	11309	5863	6619	7542	8627	9974	11236	5365	5817	6640	8014	10070	12303	5033	5403	6717	8566	11314	13251
	$10^{-8}\sigma_y^2/m^2$	4615	4172	3748	3306	2913	2628	2449	4199	3819	3509	3245	3034	2942	3943	3381	2965	2621	2332	2146	3698	2930	2267	1753	1269	1004
	$\sigma_p^2/mbar^2$	0	22	80	121	221	382	510	182	649	870	2838	5241	7988	195	646	1587	2995	4707	4813	7	35	129	135	191	260
1600	$10^{-8}\sigma_x^2/m^2$	9065	9851	11050	12723	14645	16848	18546	9250	9737	10516	11431	12408	13242	8978	9098	9204	9222	9107	9075	8175	7660	7069	6574	6088	5743
	$10^{-8}\sigma_y^2/m^2$	7943	7122	6438	5845	5356	5036	4893	7176	6576	6109	5703	5336	5115	7198	6635	6255	5893	5433	5088	7125	6324	5504	4846	4322	3946
	$\sigma_p^2/mbar^2$	0	77	144	335	1155	1970	1824	151	313	658	1473	1283	1491	34	17	66	155	255	314	5	9	36	56	88	136

The values of the variances, σ_x^2, σ_y^2, σ_z^2 or σ_p^2 of the four corner points of each initially square cluster about their centre of gravity were computed for the end of each time interval and the results are given in table 3. A selection of results is also shown in figure 8. The values of σ_x^2 rapidly increase while those of σ_y^2 decrease with time for the large clusters. The effective horizontal area $\sigma_x \sigma_y$ tends to stay constant for the first few hours and then slowly increases, σ_z^2 which is zero

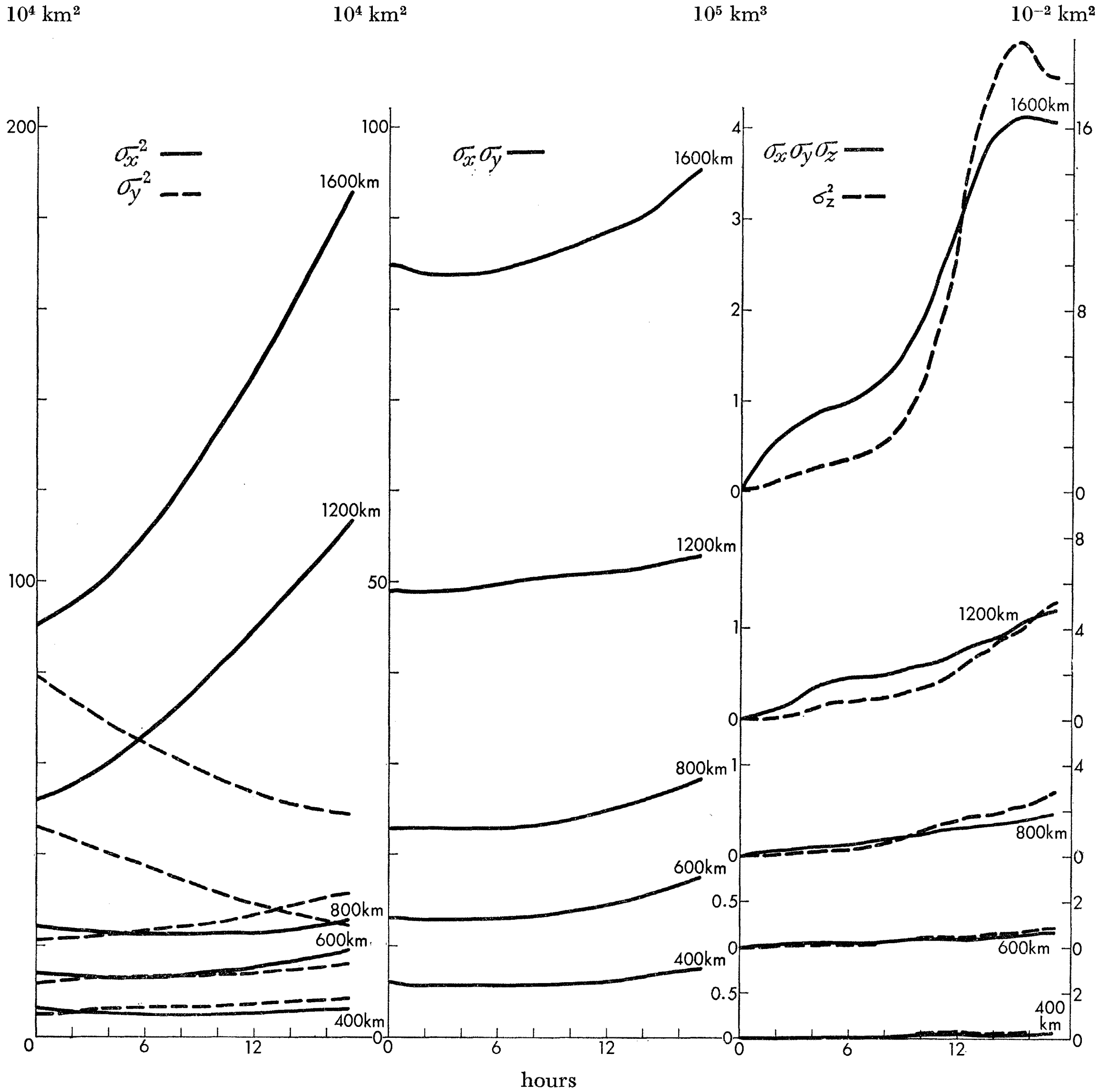

FIGURE 8. A selection of the developments of variances σ_x^2, σ_y^2, σ_z^2; areas $\sigma_x\sigma_y$; and 'volumes' $\sigma_x\sigma_y\sigma_z$ with time for clusters of different initial sizes at 900 mbar.

initially steadily increases and $\sigma_x \sigma_y \sigma_z$ increases correspondingly. The behaviour of a selection of cluster volumes formed by grid squares initially with the same (x, y) coordinates and 100 mbar thick has also been computed and the results are given in table 4. Similarly to the $\sigma_x \sigma_y$ values these are relatively constant for the first few hours and then steadily increase. Table 5 lists a selection of values of the exponent β (see (25)) computed to give an expansion law for some of the above quantities between 9 and 18 h after initiation.

PHILOSOPHICAL TRANSACTIONS OF THE ROYAL SOCIETY A MATHEMATICAL, PHYSICAL & ENGINEERING SCIENCES

In practical problems such as the dispersion of a large scale smoke pall the primary interest is probably in the rate of dispersion expressed as the variation of $(\sigma_x^2+\sigma_y^2+\sigma_z^2)$ with time. σ_z^2 is comparatively small compared to $\sigma^2 = (\sigma_x^2+\sigma_y^2)$ and values of σ^2 and $\sigma^2-\sigma_0^2$ were plotted against time on logarithmic scales in figure 9. It is clear that the initial size σ_0^2 will still be an important parameter in determining the cluster size well after the termination of the experiment. $\sigma^2-\sigma_0^2$, on the other hand, varies with t^β with β between 2 and 3, and β decreases with time. This is

TABLE 4. SOME VALUES OF $10^{-6}\,\sigma_x\,\sigma_y\,\sigma_{\Delta z}/\mathrm{km}^3$

(Δz is the depth of the 100 mbar layer Δp)

time/h ...	0	3	6	9	12	15	$17\frac{1}{4}$
approx. initial cluster side/km				Δp = 900 to 800 mbar			
200	0.06	0.06	0.06	0.06	0.06	0.07	0.08
400	—	—	—	—	—	—	—
600	0.6	0.5	0.5	0.5	0.6	0.7	0.7
800	1.0	1.0	0.9	1.0	1.1	1.1	1.2
				Δp = 700 to 600 mbar			
200	0.07	0.07	0.08	0.10	0.11	0.12	0.16
400	0.3	0.3	0.3	0.3	0.3	0.3	0.3
600	0.7	0.7	0.7	0.7	0.8	0.9	0.9
800	—	—	—	—	—	—	—
				Δp = 500 to 400 mbar			
200	0.1	0.1	0.2	0.3	0.8	1.4	1.9
400	0.5	0.4	0.4	0.5	0.8	1.1	1.3
600	1.0	1.0	1.1	1.3	1.6	1.8	3.0
800	—	—	—	—	—	—	—
				Δp = 300 to 200 mbar			
200	0.2	0.2	0.2	0.3	0.4	0.5	0.7
400	0.7	0.7	0.8	0.9	0.9	0.9	1.0
600	1.6	1.5	1.7	1.8	1.9	1.8	1.9
800	—	—	—	—	—	—	—

TABLE 5. VALUES OF THE EXPONENTS β (SEE EQUATION (25)) IN THE CLUSTER EXPERIMENT 9 TO 18 h AFTER INITIATION

	level/mbar				level/mbar			
approx. initial cluster side/km	900	700	500	300	900	700	500	300
	$\sigma_x^2+\sigma_y^2$				$(\sigma_x^2+\sigma_y^2)-(\sigma_x^2+\sigma_y^2)_0$			
100	0.8	0.4	1.5	1.5	2.1	2.0	1.5	1.7
200	0.7	1.1	1.1	2.3	3.1	2.5	1.1	3.0
400	0.5	0.2	1.2	2.3	2.7	8.2?	3.2	3.4
600	0.5	0.4	0.6	1.9	2.6	2.7	2.1	2.7
800	0.4	0.6	1.2	1.4	2.6	2.7	2.5	2.3
1200	0.6	0.6	1.3	1.0	1.8	2.2	4.1	3.3
1600	0.5	0.2	0.0	−0.5	2.1	3.1	—	—
	$\sigma_x\sigma_y$				$\sigma_x\sigma_y\sigma_p$			
100	0.8	0.6	0.3	0.4	0.8	1.1	1.4	1.5
200	1.0	0.7	2.3	7.3?	0.5	1.6	3.2	1.2
400	0.5	0.2	1.2	3.0	1.5	1.2	2.1	1.0
600	0.6	0.4	0.3	0.8	1.2	1.3	2.4	1.2
800	0.4	0.2	0.6	0.3	1.3	2.4	1.0	0.8
1200	0.1	0.3	0.4	−0.1	1.0	1.0	1.1	0.9
1600	0.2	0.1	−0.2	−0.6	1.0	1.2	0.8	0.8

PHILOSOPHICAL TRANSACTIONS OF THE ROYAL SOCIETY A MATHEMATICAL, PHYSICAL & ENGINEERING SCIENCES

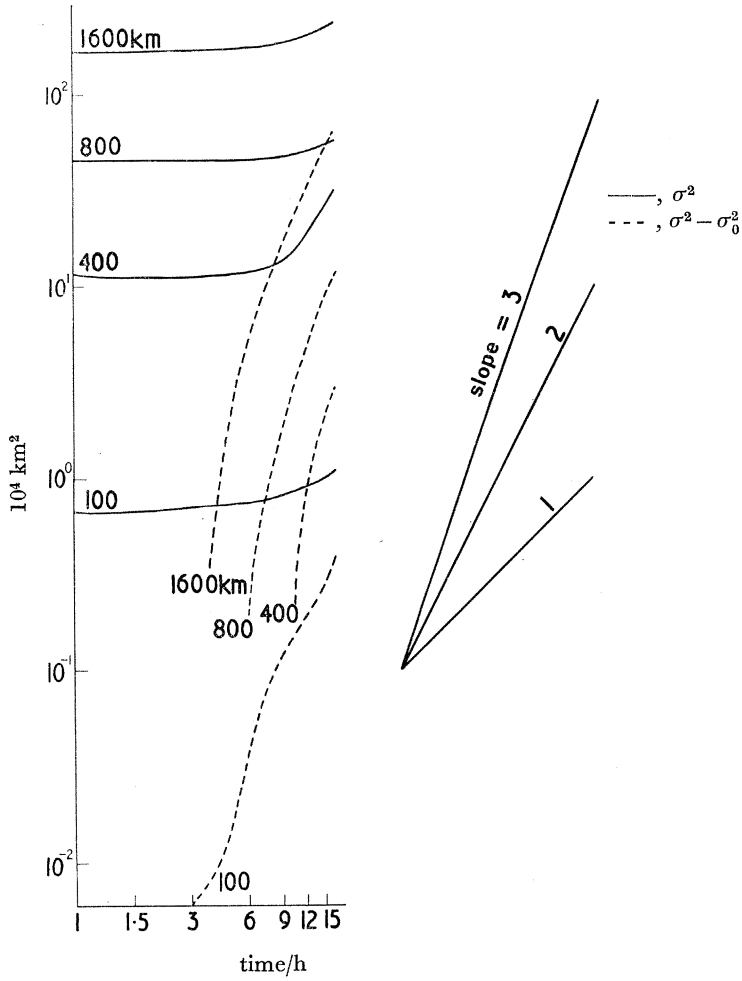

FIGURE 9. The horizontal spread of clusters $\sigma^2 = \sigma_x^2+\sigma_y^2$ and $\sigma^2-\sigma_0^2$ plotted against time on logarithmic scales for clusters of different initial sizes.

contrary to the expectations of similarity theory and indeed it is apparent from inspection of figure 7 that deformation is playing the primary role in the dispersion process in this experiment.

It is therefore of some interest whether estimates of the deformation B can be made by means of (24) using these results and the computed values are given in table 6. These are in generally good agreement with typical results calculated directly from the wind field for the general area

TABLE 6. MEAN VALUES OF DEFORMATION $10^{-5}B/\mathrm{s}^{-1}$ (SEE EQUATION (20)) CALCULATED FROM EQUATION (24) FOR THE LAST 6 h OF THE EXPERIMENT

approx. initial cluster side/km	level/mbar 900	700	500	300
100	1.6	1.1	4.8	6.3
200	1.7	1.6	4.2	6.0
400	1.0	—	1.5	3.3
600	1.2	0.8	1.3	3.4
800	1.1	0.9	2.6	3.7
1200	1.4	1.4	1.2	1.2
1600	1.3	0.4	—	—

of the clusters at the mid-time of the experiment. Further work, however, is needed to study how the effective value of the deformation depends on the length scales over which the gradients $\partial u/\partial x$ and $\partial v/\partial y$ are measured.

Conclusion

The experiment described above is preliminary in that it only extends over a comparatively short time for one synoptic situation and a small number of sequential trajectories and of clusters. A larger number of cases would be needed to obtain more definite conclusions useful for general application. One such application of this kind of work would be to use the trajectory programme in reverse, i.e. to track backwards from pollutant observations to find the source region. The advantages of using numerical models are first that they provide a method of avoiding considerable hand computations and tedious chart plotting and secondly that they are able to depict large scale vertical motions which are difficult to estimate by other methods. Further development of large scale dispersion studies using these techniques will, however, require the horizontal and vertical resolutions to be at least as good as that of the present model, a considerable extension of its global coverage and also an increase of the period for which it simulates atmospheric processes realistically to several days. There are still, however, several other difficulties and in particular the roles of deep penetrative convection and also thin inversion layers in increasing or inhibiting the large-scale dispersion require further study.

As regards the continuous point source application the present investigation confirms that, on the synoptic scale, periods of 18 h at least are still essentially in the 'small time' diffusion category. Zonal position variances are somewhat larger than the meridional values and both are 4 to 6 orders of magnitude larger than the corresponding vertical variances. In this example at least an investigation of horizontal spreads using trajectories confined to given pressure levels gave results which did not vary significantly from those due to the three-dimensional trajectories.

The study of the spreads of the clusters emphasized the importance of deformation by eddy motions on scales comparable to the cluster sizes (the approximate location of the cluster sizes investigated here relative to the overall turbulence spectrum is indicated in figure 1). The agreement between the mean deformation values computed from the rates of spread according to (24) with the directly calculated deformation fields in figure 3 is considered to be satisfactory and the dependence of rates of spread on cluster size is also well illustrated.

Acknowledgment is due to Mr F. H. Bushby for the use of the data from the Bushby–Timpson model results and to Mr G. R. R. Benwell and Miss M. R. Swann, who wrote the trajectory program used at the S.R.C. Atlas Computer Laboratory, Chilton, for helpful discussions and providing the basic trajectory information. Mr R. Smart wrote the programs used on the KDF 9 computer at the Meteorological Office, Bracknell to provide the statistical analysis of the data and with Mrs C. Siemssen who also made many hand calculations assisted greatly in the preparation of this paper. The paper is published by permission of the Director General of the Meteorological Office.

References (Murgatroyd)

Angell, J. K. 1961 *Adv. Geophys.* **8**, 138.
Angell, J. K. & Hass, W. P. 1966 *Mon. Weath. Rev., Wash.* **94**, 151.
Batchelor, G. K. 1950 *Q. Jl R. met. Soc.* **76**, 133.
Bushby, F. H. & Timpson, M. S. 1967 *Q. Jl R. met. Soc.* **93**, 1.
Davidson, B. J., Friend, J. P. & Seitz, H. 1966 *Tellus* **18**, 301.
Djuric, D. 1964 *Final Report Contract AF* 61 (052)-366. Research in Atmospheric Macroturbulence. Inst. für Met. Technische Hochschule, Darmstadt, Germany, Part C.
Djuric, D. 1966 *Q. Jl R. met. Soc.* **92**, 231.
Durst, C. S. & Davis, N. E. 1957 *Met. Mag.* **86**, 138.
Durst, C. S., Crossley, A. F. & Davis, N. E. 1959 *J. Fluid Mech.* **6**, 401.
Edinger, J. G. & Rapp, R. R. 1957 *J. Met.* **14**, 421.
Gifford, F. 1957*a* *J. Met.* **14**, 410.
Gifford, F. 1957*b* *J. Met.* **14**, 475.
Kao, S-K. 1962 *J. Geophys. Res.* **67**, 2, 347.
Kao, S-K. 1965 *Q. Jl R. met. Soc.* **91**, 10.
Kao, S-K. & Bullock, W. S. 1964 *Q. Jl R. Met. Soc.* **90**, 166.
Manabe, S. & Hunt, B. C. 1968 *Mon. Weath. Rev., Wash.* **96**, 477.
Manabe, S., Smagorinsky, J. & Stickler, R. E. 1965 *Mon. Weath. Rev., Wash.* **93**, 769.
Mesinger, F. 1965 *J. Atmos. Sci.* **22**, 479.
Mesinger, F. & Milovanovic, O. 1963 *Geofis. pura appl.* **58**, 164.
Murgatroyd, R. J. 1969*a* *Q. Jl R. met. Soc.* **95**, 40.
Murgatroyd, R. J. 1969*b* *Q. Jl R. met. Soc.* **95**, 194.
Pasquill, F. 1962 *Atmospheric diffusion.* London: Van Nostrand.
Petterssen, S. 1956 *Weather analysis and forecasting*, 2nd Edn. vol. 1. *Motion and motion systems.* New York: McGraw-Hill.
Pinus, N. Z., Reiter, E. R., Shur, G. N. & Vinnichenko, N. K. 1967 *Tellus* **19**, 206.
Reed, R. J. & German, K. E. 1965 *Mon. Weath. Rev., Wash.* **93**, 313.
Richardson, L. F. 1926 *Proc. Roy. Soc.* A **110**, 709.
Sheppard, P. A. 1963 *Rep. Progr. Phys.* **26**, 213.
Smagorinsky, J., Manabe, S. & Holloway, J. L. Jr. 1965 *Mon. Weath. Rev., Wash.* **93**, 727.
Taylor, G. I. 1921 *Proc. Lond. Math. Soc.* Ser. 2, **20**, 196.
Van der Hoven, I. 1957 *J. Met.* **14**, 160.
Vincent, D. G. 1968 *Q. Jl R. met. Soc.* **94**, 333.
Welander, P. 1955 *Tellus* **7**, 141.

PHILOSOPHICAL TRANSACTIONS OF THE ROYAL SOCIETY A MATHEMATICAL, PHYSICAL & ENGINEERING SCIENCES